Geochemistry Geophysics Geosystems G3
AN ELECTRONIC JOURNAL OF THE EARTH SCIENCES
Published by AGU and the Geochemical Society

Article
Volume 1
December 5, 2000
Paper number 2000GC000095
ISSN: 1525-2027

Geologic evidence for a mantle superplume event at 1.9 Ga

Kent C. Condie
Department of Earth and Environmental Science, New Mexico Institute of Mining and Technology, Socorro, New Mexico 87801 (kcondie@nmt.edu)

David J. Des Marais
Ames Research Center, M/S 239-4, Moffett Field, California 94035-1000 (ddesmarais@mail.arc.nasa.gov)

Dallas Abbott
Lamont-Doherty Earth Observatory, Palisades, New York 10964 (dallas@ldeo.columbia.edu)

[1] **Abstract:** Both preserved and restored areal distributions of Proterozoic marine intracratonic, passive margin, and platform sediments show a prominent peak at ~1.9 Ga, indicating that shallow marine sediments were widespread on the continents and that sea level was high at this time. The chemical index of alteration in shales deposited at this time was high, suggesting warm climates, possibly due to enhanced CO_2 levels in the atmosphere. High sea level and warms climate may also explain an abundance of black shale, banded iron formations, and shallow marine phosphate deposits and an increase in the number of occurrences and diversity of stromatolites in general and microdigitate stromatolites at 1.9 Ga. All of these observations are consistent with a 1.9-Ga superplume event. The occurrence of only a minor positive carbon isotope shift in marine carbonates at 1.9 Ga indicates that the relative rates of burial of organic and oxidized carbon remained about the same as at present. Slightly low $^{87}Sr/^{86}Sr$ isotopic ratios in seawater at 1.9 Ga reflect increased mantle input of Sr from the proposed superplume event, whereas higher ratios at 1.85–1.75 Ga may reflect increased input of continental Sr from a growing supercontinent. The first massive sulfate evaporites in the geologic record at 1.8–1.6 Ga follow the possible 1.9-Ga superplume event. This may reflect an increase in both oxidation state and carbonate deposition in the oceans as plume-related volcanism wanes.

Keywords: Mantle plumes; sea level; superplume; carbon isotopes; black shales.

Index terms: Atmosphere; oceans; geomorphology; Precambrian.

Received July 10, 2000; **Revised** November 8, 2000; **Accepted** November 8, 2000; **Published** December 5, 2000.

Condie, K. C., D. J. Des Marais, and D. Abbott, 2000. Geologic evidence for a mantle superplume event at 1.9 Ga, *Geochem. Geophys. Geosyst.*, vol. 1, Paper number 2000GC000095 [12,044 words, 7 figures, 2 tables]. Published December 5, 2000.

Theme: Geochemical Earth Reference Model (GERM) **Guest Editor:** Hubert Staudigel

1. Introduction

[2] A mantle superplume event occurs when many large plumes generated in the lower mantle rise to the base of the lithosphere in a short period of time (<100 Myr) [*Condie*, 1998]. This is similar to the usage in the work of *Larson* [1991a, 1991b], where he applied the term superplume to one or more large mantle plumes beneath the South Pacific during the mid-Cretaceous. On the basis of the distribution of ages of juvenile crust or plume-generated igneous rocks, *Condie* [1998] and *Isley and Abbott* [1999] have proposed several superplume events in the mantle during the last 3 Gyr. *Condie* [1998, 2000a] suggests that a superplume event is part of a superevent cycle, involving supercontinent formation and breakup. The formation of a supercontinent is associated with proposed superplume events at 1.9 and 2.7 Ga. In the model, superplume events are triggered by catastrophic collapse of descending slabs through the 660-km seismic discontinuity. *Greff-Lefftz and Legros* [1999] suggest that resonance between the outer core and solar tidal waves destabilizes the D″ layer above the core, leading to the episodic generation of numerous large superplumes. Whatever the triggering mechanism, superplume events occur over short periods of time and have major effects on other Earth systems.

[3] *Larson* [1991b] and *Kerr* [1998] showed that a mid-Cretaceous superplume event coincided with increases in surface temperature, deposition of black shales, a rise in sea level, elevated $\delta^{13}C$ in seawater, and a decrease in the rate of magnetic reversals. The rise in sea level is inferred in two ways: through the sedimentary record of deposition on passive margins and in craton interiors and through the record of increased production of oceanic crust. Although the increased production rate of oceanic crust has been questioned by *Hardebeck and Anderson* [1996], the effects of a Cretaceous superplume event on platform and passive margin sedimentation are undisputed. Continental flooding and passive margin sedimentation increased greatly during the Cretaceous superplume event. Because episodes of increased continental flooding are relatively well preserved in the Precambrian stratigraphic record, we suggest that they can be used to test for the occurrence of Precambrian superplume events.

[4] The increase in global temperatures during the mid-Cretaceous superplume event is largely due to an increase in atmospheric CO_2 rather than climate moderation by increased continental flooding [*Barron et al.*, 1995]. The indirect result of this increase in global temperatures is an increase in continental weathering rates, which can be assessed by looking at the chemical index of alteration (CIA) of shales. If Precambrian superplume events were accompanied by increased atmospheric CO_2, they should manifest themselves by increased CIA in shales. Because shales are relatively easy to preserve in cratonic sequences, they are likely to preserve a record of Precambrian global warming and cooling events.

[5] Because the two major superplume events proposed at 2.7 and 1.9 Ga were probably more intense than the mid-Cretaceous event [*Condie*, 1998], they also should have manifestations in the geologic record. In particular, large injections of CO_2 into the atmosphere-ocean system should be reflected in sedimentary rocks. In this paper, we evaluate and discuss geologic features in both detrital and chemical sedimentary rocks that are consistent with, or support, a superplume event at 1.9 Ga.

2. Sea Level at 1.9 Ga

[6] Models of sea level through time are diverse and depend upon assumptions, such as crustal

thickness and growth rate, freeboard (elevation of continents above mean sea level), and mantle cooling rate, none of which are well known [*Taylor and McLennan*, 1985; *Galer*, 1991; *Gurnis*, 1993; *Eriksson*, 1999; *Eriksson et al.*, 1999]. During a superplume event, sea level should rise because of isostatic uplift and thermal erosion of oceanic lithosphere above mantle plume heads [*Kerr*, 1994; *Lithgow-Bertelloni and Silver*, 1998]. Formation of oceanic plateaus and enhanced activity of ocean ridges during a superplume event also may raise sea level by displacing seawater onto continental shelves [*Larson*, 1991b]. Supercontinent formation, on the other hand, should lower sea level as mantle upwellings develop beneath supercontinents [*Gurnis*, 1993; *Condie et al.*, 2000].

[7] Although shallow marine sedimentary successions are widespread and well preserved in the Phanerozoic and Neoproterozoic, only small remnants of older successions remain in the geologic record. For this reason, it is not possible to use sequence stratigraphy to estimate sea level in rocks older than ~800 Ma [*Eriksson*, 1999].

[8] However, remnants of Mesoproterozoic and Paleoproterozoic marine platform sediments are widespread on the continents, and hence their areal distribution as a function of time yields important insight into the relative elevation of sea level with time. In this study, areas of Proterozoic marine intracratonic, passive margin, and platform sediments (hereafter referred to as intracratonic sediments) are estimated from geologic maps ranging in scale from $1:10^6$ to 1:12,000. In regions where numerous small outcrops of the same succession occur, a line is drawn around all of the outcrops, and they are scaled as one unit. One of the major problems encountered in estimating preserved areas of sediments is that of complex structure. Where sediments are strongly folded, area estimates are minimal. If structures are relatively simple (anticlines, synclines, etc.), attempts were made to estimate predeformational areal distributions by structural reconstructions. Our results, which we consider to represent minimal areas of Proterozoic and Archean intracratonic sediments, are summarized in Table 1. Also included in Table 1 are depositional ages and estimates of the error of these ages.

[9] The areal distribution of sediments from any particular tectonic setting varies with age because of the effects of erosion. *Veizer and Jansen* [1985] and *Veizer* [1988] have shown that the preservation of sediments decays exponentially with time and varies between tectonic settings. Phanerozoic intracratonic and platform sediments have a half-life of ~350 Myr and an oblivion age (life expectancy) of ~1600 Myr [*Veizer*, 1988]. Because there are numerous examples of intracratonic sediments preserved in the geologic record that are older than 1600 Ma, a longer half-life would seem appropriate for Proterozoic sediments. A more realistic half-life for Proterozoic intracratonic sediments is ~700 Myr, with a corresponding oblivion age of ~2500 Myr. In Table 1 (column 3) we have calculated the "restored" areas of the Precambrian sediments using the method of *Veizer* [1988] with a half-life of 700 Myr.

[10] The cumulative preserved area of Proterozoic marine intracratonic sediments is shown in histogram form as a function of age in Figure 1, and the restored sediment areas are shown in similar fashion in Figure 2. Both graphs show prominent peaks at 1.9–1.8 Ga and 800–600 Ma and a smaller peak at ~2.7 Ga. This strongly suggests that shallow marine sediments were more widespread on the continents at these times than at other times during the Precambrian and, by inference, that sea level was also high at these times. It is significant that the highest peak for restored

Table 1. Areas and Ages of Late Archean and Proterozoic Intracratonic Sedimentary Rocks

Location	Preserved Area, km^2	Restored Area, km^2	*t*, Ma	Age Error, Ma	References
Adelaide Basin, Australia	840,000	1,854,558	800	50	*Ambrose et al.* [1981]; *Myers et al.* [1997]
Amadeus, Australia	80,000	152,250	650	26	*Powell et al.* [1994]; *Myers et al.* [1997]
Officer Basin, Australia	60,000	114,188	650	50	*Zang* [1995]
Brigham Group, Idaho	13,900	25,176	600	50	*Smith et al.* [1994]
Pocatello, Idaho	14,000	25,357	600	50	*Link et al.* [1993]; *Smith et al.* [1994]
East Greenland	10,500	19,983	650	100	*Fairchild and Hambrey* [1995]
Nevada–California border area	187,600	333,123	580	20	*Kaufman and Knoll* [1995]
Windemere Group, western Canada	36,700	77,113	750	40	*Jefferson and Young* [1989]; *Narbonne and Aitken* [1995]
McKenzie Mountains, Northwest Territories, Canada	29,200	64,468	800	100	*Brookfield* [1994]; *Narbonne and Aitken* [1995]
Grand Canyon Supergroup, Arizona	26,400	58,286	800	20	*Link et al.* [1993]
Amundsen, Northwest Territories, Canada	23,400	51,663	800	100	*Kaufman and Knoll* [1995]
Polarisbreen Group, Svalbard	35,000	63,393	600	20	*Fairchild and Hambrey* [1984]
Varanger Peninsula, Norway	41,700	75,528	600	40	*Vidal and Moczydlowska* [1995]
Russian Platform	80,000	152,250	650	50	*Vidal and Moczydlowska* [1995]
Damara, Namibia	1,125,000	2,037,621	600	50	*Kukla and Stanistreet* [1991]
Gariep Group, South Africa	30,000	62,724	745	15	*Tankard et al.* [1982]
Nama Group, South Africa	65,000	114,284	570	25	*Gresse and Germs* [1993]
Adrar, Mauritania	112,000	259,823	850	150	*Clauer et al.* [1982]
Madina–Kouta, NW Africa	300,000	662,342	800	100	*Villeneuve* [1989]
West Congo	200,000	380,626	650	45	*Kaufman and Knoll* [1995]
Bambui Group, Brazil	50,000	105,059	750	25	*Marshak and Alkmim* [1989]; *Misi and Veizer* [1998]
La Tinta Group, southern Brazil	45,000	89,987	700	50	*Cingolani and Bonhomme* [1982]; *Brito Neves and Cordani* [1991]
Boqui–Jacadigo Groups, Bolivia	20,000	36,224	600	24	*Litherland et al.* [1986]
Espinhaco Supergroup, eastern Brazil	25,000	49,993	700	20	*Marshak and Alkmim* [1989]
Penganga Group, India	40,000	86,153	775	40	*Chaudhuri et al.* [1989]
Raipur Group, India	35,000	94,193	1000	75	*Kale and Phansalkar* [1991]
Banzhou, southern China	25,000	67,281	1000	80	*Li and McCulloch* [1996]
Sinian, southern China	100,000	190,313	650	25	*Li and McCulloch* [1996]
Bhander Group, India	58,000	156,092	1000	150	*Chakrabarti* [1990]
Dengying Formation, southern China	125,000	249,963	700	35	*Zunyi et al.* [1986]
Jixian Group, northern China	20,000	38,063	650	20	*Yun* [1985]
Huainan Group, eastern China	56,000	106,575	650	25	*Zang and Walter* [1992]
Kuruktag Suite, eastern Tarim	25,000	45,280	600	20	*Brookfield* [1994]
Turukhansk, Siberia	40,000	97,503	900	100	*Sergeev et al.* [1997]

Table 1. (*continued*)

Location	Preserved Area, km^2	Restored Area, km^2	*t*, Ma	Age Error, Ma	References
Earaheedy Group, Western Australia	100,000	633,665	1865	62	*Hynes and Gee* [1986]; *Myers et al.* [1997]
Hatches Creek Group, central Australia	50,000	277,195	1730	22	*Blake et al.* [1987]; *Myers et al.* [1997]
Glengarry Group, Western Australia	28,000	183,682	1900	85	*Myers et al.* [1997]
Pine Creek basin, northern Australia	80,000	524,805	1900	65	*Pagel et al.* [1984]; *Needham et al.* [1988]
Reynolds Range, central Australia	50,000	297,086	1800	65	*Dirks and Norman* [1992]
Flinton Group, eastern Canada	16,700	49,621	1100	30	*Moore and Thompson* [1980]
Sibley Group, Canada	34,750	113,998	1200	100	*Ojakangas and Morey* [1982]
Athabasca Group, northern Canada	43,000	231,412	1700	100	*Ramaekers* [1981]; *Kotzer and Kyser* [1995]
Belt Supergroup, Montana	82,600	330,303	1400	75	*Link et al.* [1993]
Apache Group, Arizona	42,000	124,795	1100	100	*Link et al.* [1993]
Sioux–Barboo Qtzt, north central United States	144,500	777,652	1700	125	*Greenberg and Brown* [1984b]; *Holm* [1997]
Ortega Qtzt, New Mexico	90,350	486,234	1700	80	*Soegaard and Eriksson* [1989]
Mazatzal Group, Arizona	16,700	89,874	1700	10	*Doe and Karlstrom* [1991]
Hembrillo succession, New Mexico	18,350	98,754	1700	30	*Alford* [1987]
Ramah Group, Labrador	17,800	116,769	1900	25	*Knight and Morgan* [1981]
Marquette Supergroup, Minnesota	34,200	247,702	2000	75	*Greenberg and Brown* [1984a]
Animikie Group, Minnesota	26,100	189,036	2000	100	*Van Schmus* [1976]; *Sims et al.* [1993]
Mistassini Group, eastern Canada	13,300	91,676	1950	35	*Rivers* [1997]
Kaniapiskau Group, eastern Canada	25,000	164,002	1900	150	*Rivers* [1997]
Belcher Group, Canada	123,800	812,136	1900	150	*Donaldson and Ricketts* [1979]; *Hoffman* [1988]; *Chandler and Parrish* [1989]
Goulburn–Bear Creek, Canada	39,800	277,069	1960	50	*Campbell* [1979]; *Hoffman* [1988]
Great Slave Supergroup, Canada	58,380	382,976	1900	50	*Hoffman* [1988]
Coronation Supergroup, Canada	44,480	291,792	1900	40	*Hoffman* [1988]
Baker Lake, Canada	13,900	86,781	1850	50	*Aspler and Chiarenzelli* [1997]
Amer Group, Canada	6100	38,084	1850	20	*Hoffman* [1988]
Fox River, Canada	26,270	168,954	1880	10	*Hoffman* [1988]
Wollaston, Canada	44,480	277,700	1850	25	*Hoffman* [1988]
Yurmata Group, Russia	60,000	217,314	1300	40	*Sergeev* [1994]
Burzyan Group, Russia	40,000	194,977	1600	50	*Sergeev* [1994]
Ruzizian, Congo	75,000	543,206	2000	100	*Mendelsohn* [1981]
Toro Group, Uganda	25,000	164,002	1900	100	*Goodwin* [1991]
Mporokoso Group, Zambia	50,000	269,084	1700	50	*Unrug* [1984]
Jacobina Group, eastern Brazil	10,500	76,049	2000	100	*Ledru et al.* [1997]
Roraima Supergroup, Guiana	132,000	710,381	1700	100	*Gibbs and Barron* [1993]

Table 1. (*continued*)

Location	Preserved Area, km^2	Restored Area, km^2	*t*, Ma	Age Error, Ma	References
Vaupes Supergroup, Guiana	67,000	295,803	1500	60	*Gibbs and Barron* [1993]
Rio Fresco, Brazil	110,000	666,660	1820	100	*Bonhomme et al.* [1982]; *Teixeira et al.* [1989]
Beneficiente Group, northern Brazil	113,750	527,687	1550	75	*Bonhomme et al.* [1982]; *Teixeira et al.* [1989]
San Ignacio Group, Bolivia	200,000	848,710	1460	100	*Litherland et al.* [1986]
Paranoa Group, India	30,000	89,139	1100	50	*Fairchild et al.* [1996]
Cuddapah Supergroup, southern India	65,000	349,809	1700	50	*Meijerink et al.* [1984]; *Kale and Phansalkar* [1991]
Kaladgi Group, India	10,000	53,817	1700	150	*Kale and Phansalkar* [1991]
Purana basins, India	90,000	359,894	1400	100	*Kumar* [1995]; *Kale and Phansalkar* [1991]
Vindhyan Supergroup, India	90,000	295,246	1200	50	*Kumar* [1995]; *Kale and Phansalkar* [1991]
Gangpur Group, India	7,500	38,988	1665	25	*Kumar* [1995]; *Kale and Phansalkar* [1991]
Sibao Group, southern China	25,000	95,143	1350	40	*Li and McCulloch* [1996]
Liaohe Group, northern China	42,000	289,504	1950	40	*Zunyi et al.* [1986]
Changchengian Formation, northern China	25,550	159,515	1850	75	*Zunyi et al.* [1986]
Derbina sequence, Siberia	25,000	115,975	1550	150	*Rosen et al.* [1994]
Pahrump Group, California	15,300	44,570	1080	20	*Wright et al.* [1974]; *Heaman and Grotzinger* [1992]
St. Boniface Group, eastern Canada	4000	12,738	1170	30	*Rivers* [1997]
Osler Group, eastern Canada	23,000	71,808	1150	30	*Ojakangas and Morey* [1982]
Mount Isa Supergroup, NE Australia	50,000	284,142	1755	35	*Blake and Stewart* [1992]
McArthur Early, northern Australia	180,000	1,017,859	1750	10	*Rawlings* [1999]
McArthur Intermediate, northern Australia	45,000	230,480	1650	15	*Rawlings* [1999]
McArthur Late, northern Australia	80,000	336,140	1450	10	*Rawlings* [1999]
Bangemall Early, Western Australia	30,000	148,420	1615	15	*Collins and McDonald* [1994]; *Myers et al.* [1997]
Bangemall Late, Western Australia	30,000	117,032	1375	100	*Collins and McDonald* [1994]; *Myers et al.* [1997]
Birrindudu basin, northern Australia	25,000	118,294	1570	20	*Sweet* [1977]; *Myers et al.* [1997]
Yeneena Supergroup, NW Australia	66,000	216,514	1200	120	*Williams* [1990]; *Myers et al.* [1997]
Victoria River basin, northern Australia	35,000	114,818	1200	50	*Tyler and Griffin* [1990]; *Myers et al.* [1997]
Hurwitz Group, Canada	112,600	994,104	2200	100	*Hoffman* [1988]
Black Hills, South Dakota	36,700	272,470	2025	20	*Hoffman* [1988]
Snowy Pass Supergroup, Wyoming	68,700	669,646	2300	75	*Hills and Houston* [1979]; *Karlstrom et al.* [1983]
Huronian Supergroup, eastern Canada	110,000	1,072,213	2300	75	*Fedo et al.* [1997]; *Rivers* [1997]
Otish Group, eastern Canada	16,100	164,897	2350	50	*Rivers* [1997]
Lomagundi Group, Zimbabwe	15,000	119,947	2100	100	*Cahen and Snelling* [1984]; *Master* [1991]

Table 1. (*continued*)

Location	Preserved Area, km^2	Restored Area, km^2	*t*, Ma	Age Error, Ma	References
Piriwiri Group, Zimbabwe	35,000	253,496	2000	75	*Cahen and Snelling* [1984]; *Master* [1991]
Central Finland	54,000	526,359	2300	100	*Melezhik et al.* [1997]
Minas Supergroup, Brazil	10,800	118,551	2420	25	*Babinski et al.* [1995]; *Machado et al.* [1996]
Prince Charles Land, Antarctica	100,000	1,311,819	2600	50	*Sheraton et al.* [1987]
Aravalli Group, India	30,000	374,540	2550	50	*Verma and Greiling* [1995]; *Wiedenbeck et al.* [1996]
Sandur Schist, India	35,000	415,860	2500	50	*Manikyamba and Naqvi* [1995]
Chitradurga Group, southern India	25,000	327,955	2600	100	*Argast and Donnelly* [1986]
Hutuo Group, northern China	30,000	378,266	2560	50	*Wang and Qiao* [1984]
Shuanshanzi Group, northern China	30,000	239,894	2100	100	*Zunyi et al.* [1986]
Wutai Group, northern China	25,000	297,043	2500	100	*Zunyi et al.* [1986]
Hamersley Supergroup, Western Australia	50,000	594,085	2500	80	*Trendall* [1983]; *Myers et al.* [1997]
Turee Creek–Wyloo Groups, Western Australia	35,000	309,002	2200	95	*Thorne and Seymour* [1991]; *Myers et al.* [1997]
Yerrida Group, Western Australia	75,000	662,147	2200	110	*Pirajno et al.* [1996]; *Myers et al.* [1997]
Hapschan Series, Siberia	50,000	538,088	2400	150	*Condie et al.* [1991]
Udokan Series, Siberia	45,000	397,288	2200	100	*Rosen et al.* [1994]
Dzheltulak Group, Siberia	30,000	252,068	2150	50	*Rosen et al.* [1994]
Zhongtiao Group, northern China	15,000	119,947	2100	50	*Sun et al.* [1990]
Transvaal Supergroup, South Africa	105,000	1,223,120	2480	50	*Eriksson and Clendenin* [1990]; *Cheney and Twist* [1986]
Witwatersrand Supergroup, South Africa	37,500	662,050	2900	40	*Robb et al.* [1990]; *Winter* [1994]
Pongola Supergroup, South Africa	28,800	528,993	2940	60	*Cheney and Winter* [1995]
Francevillian Supergroup, Gabon	37,500	299,868	2100	65	*Ledru et al.* [1989]
Jatulian successions, Finland	25,000	199,912	2100	55	*Heiskanen* [1991]

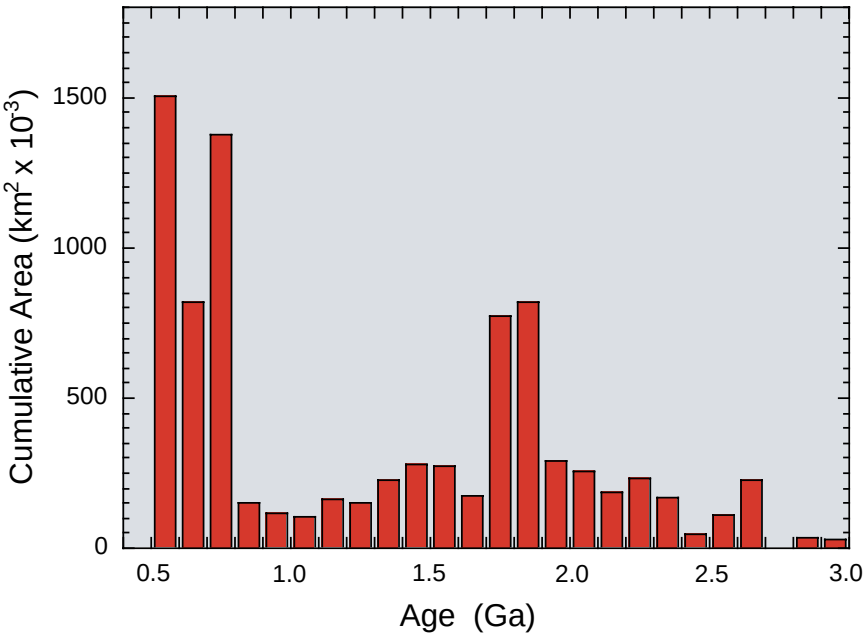

Figure 1. Histogram showing the cumulative aerial distribution of preserved intracratonic, passive margin, and platform sediments during the Precambrian. Data are from Table 1.

intracratonic sediment occurs at ~1.9 Ga (Figure 2). Better resolution of these peaks must await more precise dating of the sedimentary successions.

[11] Also supporting a high sea level at ~1.9 Ga is the widespread occurrence of submarine flood basalts of this age erupted on continental platforms. Many examples of such basalts occur in the circum-Superior orogen in Quebec, in the Birrimian in West Africa, and on the Baltic shield in Scandinavia [*Arndt*, 1999]. This suggests that continental shelves were extensively inundated at 1.9 Ga.

[12] A high sea level at 1.9 Ga is consistent with a superplume event at this time, as proposed by *Condie* [1998, 2000a]. The decrease in sea level after 1.85 Ga recorded by a decrease in preserved intracratonic sediments may reflect the formation of a supercontinent that followed and partially overlapped a superplume event [*Condie*, 2000b]. This is consistent with the timing of events within the superevent cycle suggested by *Condie* [1998].

3. Paleoclimate

[13] The chemical index of alteration (CIA), or paleoweathering index [*Nesbitt and Young*, 1982; *Nesbitt et al.*, 1996], has been used to estimate the degree of chemical weathering in the source areas of shale. The CIA is calculated from the molecular proportions of oxides, where CaO is the amount in only the silicate fraction and CIA equals the $[Al_2O_3/(Al_2O_3 + CaO + Na_2O + K_2O)] \times 100$ molecular ratio. The higher the CIA, the greater the degree of chemical weathering in sediment sources. For example, CIA values over 85 are characteristic of residual clays in tropical climates, and [*Nesbitt and Young*, 1982]. Although CIA data show considerable scatter in some stratigraphic sections, due perhaps to later remobi-

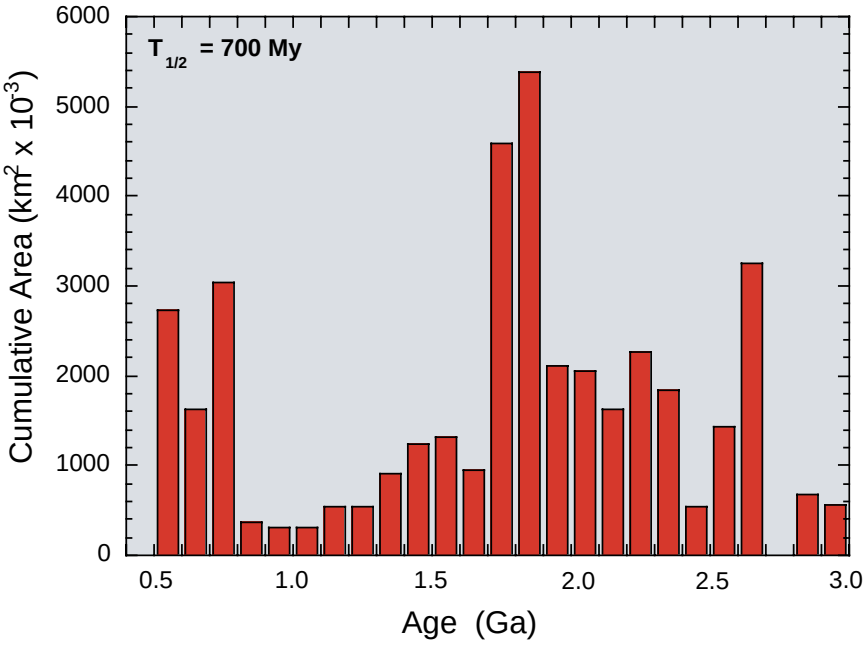

Figure 2. Histogram showing the restored aerial distribution of intracratonic, passive margin, and platform sediments during the Precambrian. Data are from Table 1. The area was restored using a sediment half-life of 700 Myr and the exponential decay relation given by *Veizer* [1988].

lization of Ca, Na, or K, results indicate a major peak in CIA values of shales at ~1.9 Ga and another at 1.7 Ga [*Condie and Des Marais*, 1999; *Condie et al.*, 2000] (Figure 3). The peaks in CIA at 1.9 and 1.7 Ga suggest that paleoclimates were unusually warm at these times, a feature consistent with increased input of greenhouse gases (principally CO_2) into the atmosphere. This is to be expected during superplume events.

[14] The origin and significance of the 1.7-Ga peak in CIA is not well understood. The fact that it correlates with intracratonic sediment and black shale peaks at about the same time (Figure 3) indicates a warm climatic regime with relatively high sea level at 1.7 Ga. *Isley and Abbott* [1999] have proposed another superplume event at ~1.7 Ga, and the sediment and CIA peaks seem to support the existence of such an event.

4. Banded Iron Formation (BIF)

[15] BIFs are finely laminated, chemical sediments composed chiefly of microcrystalline quartz and iron oxides. The most voluminous BIFs (Superior type) were deposited in intracratonic, passive margin, or platform basins during stands of high sea level during the late Archean and Paleoproterozoic [*Simonson and Hassler*, 1996]. The iron and silica in BIFs appear to have been derived from hydrothermal vents on the deep seafloor, and their deposition on shallow continental shelves and intracratonic basins requires one of two processes: (1) upwelling, which brings iron-rich waters from the largely anoxic deep basins into the oxidizing shallow water on the continents [*Klein and Beukes*, 1992], or (2) extensive hydrothermal plumes, depleted in oxygen and enriched in iron, associated with either or both ocean ridge systems or oceanic plateaus [*Isley*,

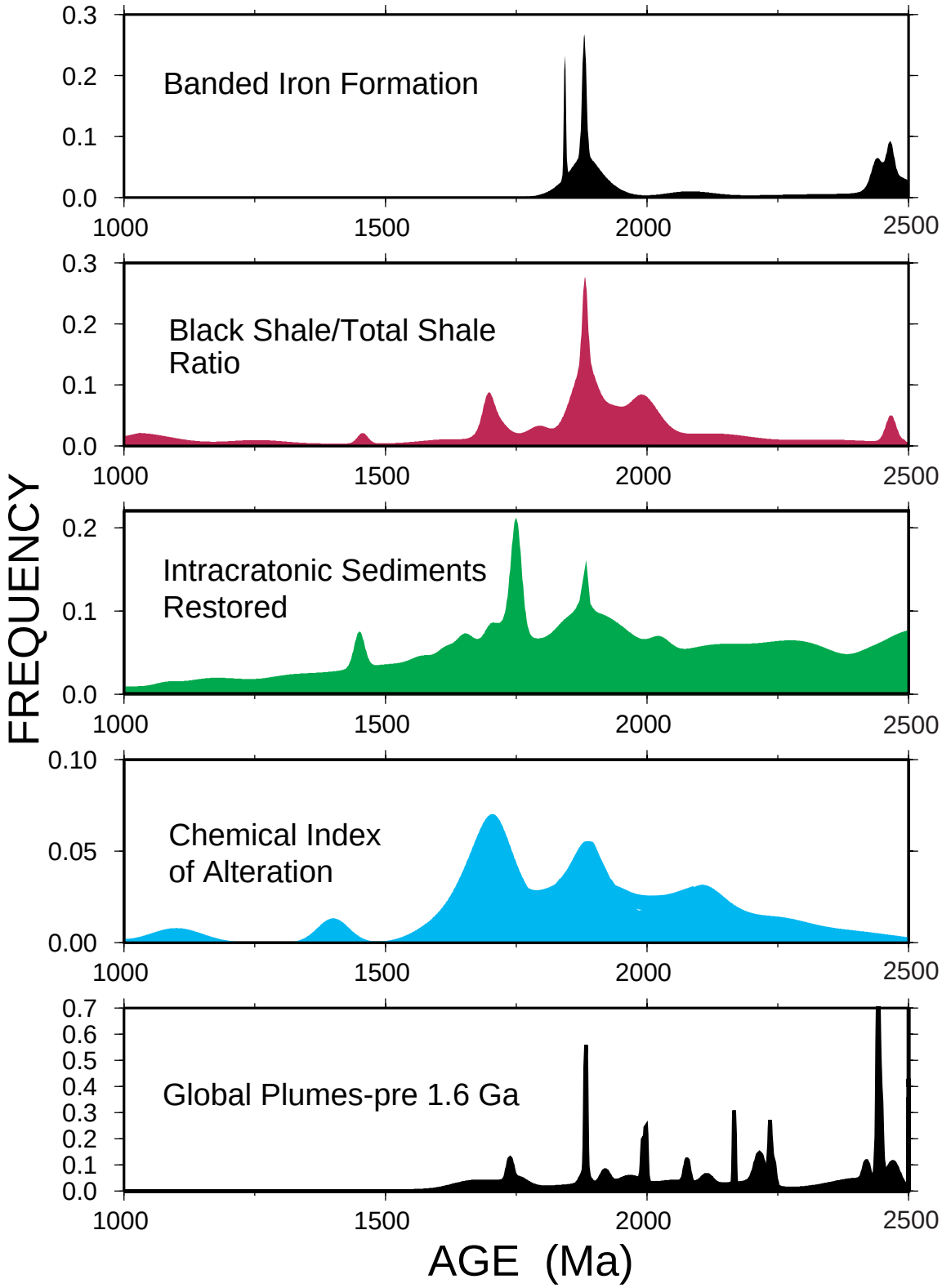
Banded Iron Formation
Black Shale/Total Shale Ratio
Intracratonic Sediments Restored
Chemical Index of Alteration
Global Plumes-pre 1.6 Ga
FREQUENCY
AGE (Ma)
1000
1500
2000
2500

1995]. In the latter case, the hydrothermal plumes transport iron into the upper water column as they rise to a level of neutral buoyancy and spread outward because of ocean currents. In this manner the iron is carried onto continental shelves where BIF is deposited.

[16] The last major period of BIF deposition was at ~1.9 Ga, when the large BIFs of Labrador Trough in northern Quebec, the Animikie basin in Minnesota, and the Nabberu basin in Western Australia were deposited [*Klein and Beukes*, 1992]. As shown by *Isley and Abbott* [1999], this last peak in BIF deposition correlates well with a proposed 1.9-Ga superplume event and suggests a cause and effect relationship (Figure 3). A similar correlation with a superplume event has been suggested for the voluminous BIFs at ~2.5 Ga [*Barley et al.*, 1997; *Isley and Abbott*, 1999].

[17] A superplume event can account for several features of BIF deposition. First, the enhanced submarine volcanism and hydrothermal venting associated with both ocean ridge and oceanic plateau volcanism during a superplume event may be the source of the iron and silica in BIF. Furthermore, the elevated sea level caused by a superplume event, as discussed previously, provides extensive shallow marine basins along stable continental platforms, necessary to preserve BIF against later subduction. This applies to either the upwelling or hydrothermal plume models of deposition. The end of the BIF event at 1.9 Ga may be related to either of or, more likely, a combination of the following: (1) a decrease in concentration of ferrous iron in the oceans, a feature resulting from decreasing amounts of submarine hydrothermal activity as a superplume event declines in intensity, or (2) increasing oxygenation of deep ocean waters including, perhaps, introduction of dense plumes of sulfate-rich water. After 1.8 Ga the effects of oxygenic photosynthesis, together with organic burial and a weaker hydrothermal flux, led to global sulfate deposition and to the complete disappearance of BIF. It would appear that later superplume events, including a possible event at 1.7 Ga, were insufficient to reinitiate deposition of BIF.

5. Sedimentary Phosphates

[18] In many respects, what we know about the deposition of BIF also applies to many sedimentary marine phosphates. The main difference between the environments of deposition is that phosphates are deposited in biologically productive upwelling zones, whereas BIFs are not. For marine phosphate deposition we need a source of phosphorus, relatively anoxic seawater to keep the phosphorus in solution, and upwelling along continental margins (or hydrothermal plumes), which brings phosphorus-rich seawater onto continental shelves and basins that contain oxidizing water and biologic activity where phosphates can be precipitated [*Cook and Shergold*, 1984, 1986].

[19] Although sedimentary phosphates do not become widespread until after ~800 Ma, some important deposits occur in the Paleoprotero-

Figure 3. Time series of BIF, black shale, CIA in intracratonic shales, and restored intracratonic sediments in the Proterozoic compared with the distribution of global plumes from *Isley and Abbott* [1999]. Time series were generated by summing Gaussian distributions of unit area using mean ages and standard deviations given by *Condie et al.* [2000]. CIA equals the $[Al_2O_3/(Al_2O_3 + CaO + Na_2O + K_2O) \times 100]$ molecular ratio, with CaO representing the silicate fraction only. CIA values are given by *Condie et al.* [2000]. In the time series, CIA represents a sum of normal distributions whose height is determined by the error in the age of the CIA determination and the value of CIA. The relation of CIA to peak height is given approximately by CIA = 38.0 + 738 times peak height.

zoic [*Cook and McElhinny*, 1979]. These are in Australia in the Rum Jungle (1.9 Ga) and Broken Hill (1.9–1.8 Ga) areas, in the Animikie/Gunflint successions in Minnesota (~1.9 Ga), in the Vayrylankyla area of Finland (2.0–1.9 Ga), and in the Yenisey province of Siberia (1.85 Ga) [*Cook and McElhinny*, 1979; *Needham et al.*, 1988; *Rosen et al.*, 1994; *Nutman and Ehlers*, 1998]. These phosphates were deposited at or near 1.9 Ga and hence may correlate with the proposed 1.9-Ga superplume event. The source of the increased phosphorus and widespread anoxia in seawater at this time could be from submarine hydrothermal systems associated with the superplume event. This model also explains the association of some phosphates with BIFs, in that dissolved phosphate is strongly absorbed on ferric oxides under aerobic conditions [*Berner*, 1999].

6. Sr Isotopes in Seawater

[20] *Veizer and Compston* [1976] were the first to suggest that the growth rate of continental crust can be tracked with Sr isotopes using the $^{87}Sr/^{86}Sr$ ratio of marine carbonates. Because the $^{87}Sr/^{86}Sr$ ratio of marine carbonates reflects chiefly the balance of Sr contributed from continental versus deep-sea hydrothermal sources [*Veizer*, 1989; *Asmerom et al.*, 1991], relatively high $^{87}Sr/^{86}Sr$ ratios indicate sources with high Rb/Sr ratios (continental crust), whereas low ratios reflect dominant mantle input. Prior to ~2.5 Ga, $^{87}Sr/^{86}Sr$ ratios fall near the mantle growth curve (~0.702), indicating that the oceans were largely buffered by mantle input and that little continental crust existed, at least above sea level [*Veizer and Compston*, 1976]. After a major period of continental crustal growth and emergence above sea level at 2.7–2.6 Ga [*Veizer and Compston*, 1976; *Taylor and McLennan*, 1985; *Condie*, 1998], however, the $^{87}Sr/^{86}Sr$ ratio in seawater increased rapidly as increased amounts of continental Sr entered the oceans.

[21] In the Paleoproterozoic the $^{87}Sr/^{86}Sr$ ratio in some of the least radiogenic marine carbonates (such as those from the Albanel Formation in Quebec (1.85 Ga) and the McArthur Group in northern Australia (1.75 Ga)) increased to values near 0.706, whereas in slightly older carbonates the ratio remained relatively low (0.704) (for example, in the Coronation Supergroup in Canada (1.9 Ga)) near the mantle growth curve [*Mirota and Veizer*, 1994]. Perhaps the relatively low $^{87}Sr/^{86}Sr$ ratios in seawater at 1.9 Ga reflect increased mantle input of Sr from the proposed superplume event at this time, whereas the higher ratios at 1.85–1.75 Ga reflect increased input of continental Sr from a growing supercontinent [*Condie*, 1998]. If there was a superplume event at 1.9 Ga, why did it not decrease seawater Sr isotope ratios to even lower values? One possible reason is the large volume of continental crust formed at 2.7 Ga, which, even during a 1.9-Ga superplume event, continued to supply significant amounts of continental Sr to the oceans. Intermediate $^{87}Sr/^{86}Sr$ ratios in Mesoproterozoic marine carbonates (~0.705) correlate with supercontinent stasis, and perhaps with minor breakup at 1.5–1.4 Ga [*Condie*, 2000c].

7. Stromatolites

[22] Stromatolites, layered structures thought to be deposited by microbial mat communities, are widespread in the Proterozoic with a prominent peak (or peaks) in distribution at ~1.9–1.8 Ga. Maxima at this time occur in the number of stromatolite occurrences, in the diversity of stromatolites, and in the number of occurrences of microdigitate stromatolites [*Grotzinger and Kasting*, 1993; *Hofmann*, 1998] (Figure 4). Other investigators have not recognized this peak because data were averaged over long time intervals [*Awramik*, 1992; *Semikhatov and Raaben*, 1996]. In addition to stromatolites there are maxima in the reported occurrences of microfossils, oncoids, and che-

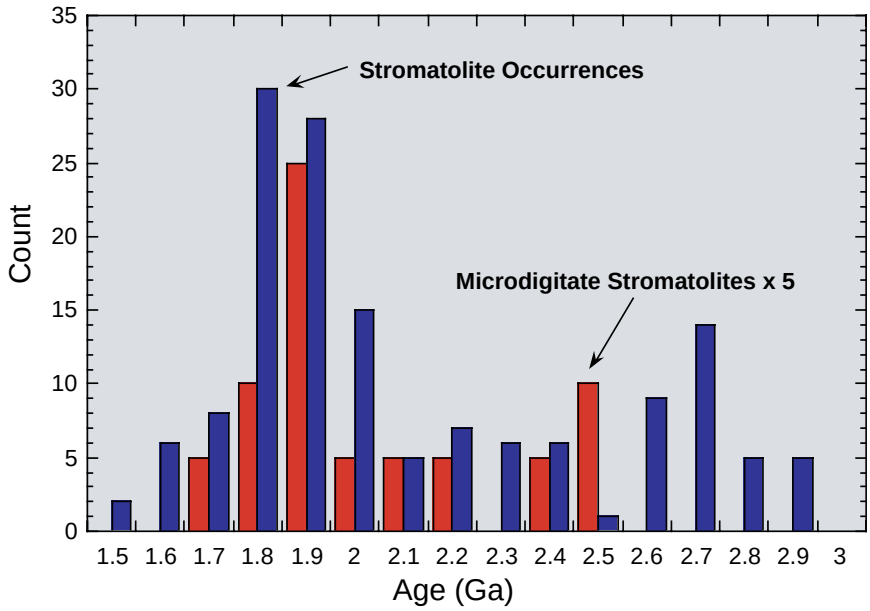

Figure 4. Distribution of reported number of occurrences of total stromatolites and of microdigitate stromatolites during the Precambrian. Data are from *Grotzinger and Kasting* [1993] and *Hofmann* [1998].

mofossils (biogenic chemical remains) at ~1.9 Ga [*Hofmann*, 1998]. The peaks in abundance and diversity of these fossils at ~1.9 Ga may reflect a combination of global warming, high sea level stands, and enhanced input of CO_2 into the sedimentary cycle. All of these may be related to a superplume event at 1.9 Ga. *Grotzinger and Knoll* [1999] suggest that the degree of carbonate saturation in seawater may be very important in controlling stromatolite diversity, and during superplume events, seawater carbonate saturation may increase significantly. Thus a superplume event may increase both the availability of carbonate and the proportion of shallow platforms for the deposition and preservation of carbonates.

[23] The distribution of Paleoproterozoic carbonates indicates that cement crusts, and, in particular, microdigitate stromatolites deposited in tidal flats, were a common mode of deposition of calcium carbonate during the Paleoproterozoic [*Grotzinger and Kasting*, 1993]. This feature appears to require Proterozoic seawater that was greatly oversaturated in $CaCO_3$ compared to Phanerozoic seawater. The peak in reported occurrences of microdigitate stromatolites at ~1.9 Ga (Figure 4) is particularly intriguing in that it correlates with the suggested superplume event at this time. This is consistent with enhanced CO_2 input into the oceans from submarine volcanism and hydrothermal vents accompanying the superplume event, because higher CO_2 means an increase in the HCO_3/SO_4 ratio in seawater, favoring deposition of carbonate over sulfate. Also, high sea level stands create widespread shallow tidal flats where both Ca and HCO_3 ions increase in concentration in seawater because of evaporation.

8. Massive Sulfate Evaporites

[24] The first massive sulfate evaporites in the geologic record occur at 1.8–1.6 Ga, following a possible 1.9-Ga superplume event (Figure 5).

Figure 5. Distribution of massive sulfate evaporites during the Precambrian. Data are from *Grotzinger and Kasting* [1993] and miscellaneous sources.

The fact that widespread sulfate deposition followed a 1.9-Ga superplume event is consistent with the following sequence of events: (1) Large amounts of sulfur were injected into the oceans as sulfide during the superplume event, but only some of the sulfur was deposited as iron sulfides on the deep seafloor [*Canfield*, 1998]; (2) the oceans became oxic as submarine volcanic input related to the superplume event subsided; and (3) as carbonate levels decreased in seawater because of falling CO_2 input from the superplumes, marine carbonate deposition became less important and Ca^{++} ion became available to precipitate as sulfates [*Grotzinger and Kasting*, 1993]. Increasing levels of sulfate in the oceans at this time are also supported by sulfur isotopes in which the range of $\delta^{34}S$ increases (less than -20 to greater than +20) after 2.2 Ga [*Canfield*, 1998]. Also, the completion of a supercontinent at this time may have provided numerous partially closed basins for evaporite deposition, as it did on Pangea during the Permian and Triassic.

[25] Alternatively, the sulfate, black shale, and CIA peaks at 1.7 Ga may reflect another superplume event at this time, with all of these peaks recording widespread global warming. If so, why is there no evidence of sulfate evaporite deposition corresponding to possible superplume events at 2.7 and 1.9 Ga? There probably was not enough oxygen available to oxidize sulfur at 2.7 Ga. However, by 1.9 Ga, this should not have been a problem. If there was a 1.7-Ga superplume event, for some reason it must have caused more global warming than the 1.9-Ga event, thus leading to widespread sulfate deposition.

9. Black Shales and Carbon and Sulfur Isotopes

[26] There is a good correlation between a 1.9-Ga superplume event and the distribution of black shales, expressed either as total cumulative thickness or as the black shale/total shale

ratio (Figure 3) [*Condie and Des Marais*, 1999; *Condie et al.*, 2000]. The black shale and CIA peaks may reflect the combined effects of mantle superplume events and supercontinent formation, the former of which introduced massive amounts of CO_2 into the atmosphere-ocean system, increasing depositional rates carbon and increasing global warming. Increased black shale deposition at these times is due to some combination of (1) increased oceanic hydrothermal fluxes (introducing nutrients), (2) anoxia driven onto continental shelves, and (3) disrupted ocean currents.

[27] The impact of a superplume upon the biogeochemical cycles of carbon and sulfur can be explored further by considering their stable isotopic records. These cycles consist of elemental reservoirs linked by processes that either transport or chemically transform these elements. Carbon and sulfur enter the surface environment by both weathering and thermal processes (i.e., volcanism, hydrothermal activity, and metamorphism). These elements are then rapidly cycled through the biosphere, which converts a fraction of their flows to reduced species by utilizing reducing power provided by weathering, thermal sources, and oxygenic photosynthesis. The amounts of organic carbon, carbonate, sulfides, and sulfate buried depend upon both the elemental fluxes through the surface environment and the burial rates in a range of sedimentary environments that favor sedimentation of either oxidized or reduced species. For example, the burial of both reduced carbon and sulfides is favored by reducing marine environments [*Berner*, 1983].

[28] The cycling of carbon can be monitored via an isotopic mass balance [*Des Marais et al.*, 1992]:

$$\delta_{Cin} = f_{carb}\delta_{carb} + f_{org}\delta_{org}, \quad (1)$$

where δ_{Cin} is the mean isotopic composition of carbon entering the surface environment. The right side of the equation represents the weighted-average isotopic composition of carbonate ($\delta^{13}C_{carb}$) and organic ($\delta^{13}C_{org}$) carbon being buried, and f_{carb} and f_{org} represent the fractions of carbon buried in each form ($f_{carb} = 1\ f_{org}$). Over timescales of >100 Myr, $\delta_{in} = 5\%$, the average value for crustal carbon [*Holser et al.*, 1988]. Thus, where values of sedimentary δ_{carb} and δ_{org} can be measured, it is possible to determine f_{carb} and f_{org} for ancient carbon cycles. For example, lower values of $\delta^{13}C_{carb}$ and/or $\delta^{13}C_{org}$ indicate higher values of f_{carb}.

[29] A similar mass balance equation applies for sulfur, as follows:

$$\delta_{Sin} = f_{SO4=}\delta_{SO4=} + f_{Sred}\delta_{Sred}, \quad (2)$$

where δ_{Sin} represents the isotopic composition of sulfur entering the surface environment. The right side of the equation represents the weighted-average isotopic composition of sulfate ($\delta^{34}S_{SO4=}$) and sulfides ($\delta^{34}S_{Sred}$) being buried, and $f_{SO4=}$ and f_{Sred} represent the fractions of sulfur buried in each form ($f_{SO4=} = 1 - f_{Sred}$). Over timescales of >100 Myr, $\delta_{in} = 0\%$, the average value for crustal sulfur [*Holser et al.*, 1988]. Thus, for example, lower values of $\delta^{34}S_{Sred}$ indicate higher values of $f_{SO4=}$.

[30] The Paleoproterozoic interval witnessed large global excursions in $\delta^{13}C_{carb}$ values (Figure 6). The very positive $\delta^{13}C_{carb}$ values situated between 2.44 and 2.39 Ga and between 1.92 and 1.97 Ga each represent only single sedimentary basins, and therefore it is not yet established that they record global-scale phenomena [*Melezhik et al.*, 1999; *Buick et al.*, 1998]. However, each of the positive and negative isotopic excursions between 2.3 and 2.0 Ga are documented within multiple basins and very likely represent widespread events [*Melezhik et al.*, 1999]. If these $\delta^{13}C_{carb}$ values reflect global excursions in $\delta^{13}C_{inorganic}$ values of Paleoproterozoic seawater, then the fraction of carbon buried as organic matter (f_{org}) varied

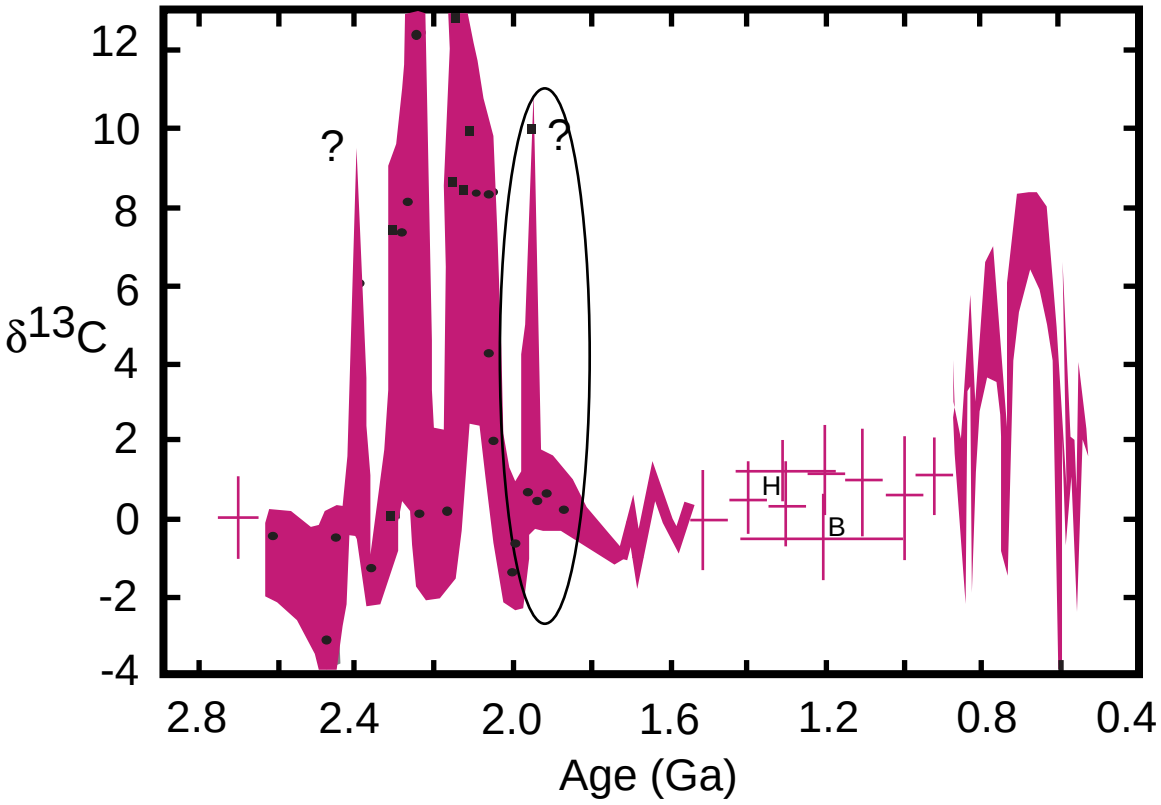

Figure 6. Carbon isotopic composition ($\delta^{13}C_{carb}$) of Proterozoic carbonates versus age (Ga). Data are from the following sources: Each data point within the shaded area between 2.7 and 1.65 Ga represents an average of multiple analyses (see reviews by *Karhu and Holland* [1996] and *Melezhik et al.* [1999]); unmarked crosses both at 2.7 Ga and between 1.7 and 0.9 Ga are 100-Ma running averages of data compiled by *Des Marais* [1997]; section between 1.7 and 1.5 Ga is from *Brasier and Lindsay* [1998]; data labeled "H" and "B" are from *Hall and Veizer* [1996] and *Buick et al.* [1995], respectively; the shaded field of data between 0.5 and 0.85 Ga is from a review by *Kaufman and Knoll* [1995]. Question marks highlight data points that represent single basins only and therefore might reflect only regional, rather than global, isotopic excursions [see *Melezhik et al.*, 1999]. The oval encloses data representing the period surrounding the proposed 1.9-Ga superplume event.

repeatedly from less than 20% to more than 50% of the global carbon flux [*Karhu and Holland*, 1996]. However, at least some of the most positive $\delta^{13}C_{carb}$ values apparently developed within large hypersaline, restricted basins that also sustained abundant stromatolite growth [*Melezhik et al.*, 1999]. During the proposed 1.9-Ga superplume event, moderately positive $\delta^{13}C_{carb}$ values indicate that f_{org} was slightly higher than its long-term global average value, consistent with the observed abundance peak in black shales. Remarkably, after 1.92 Ga, $\delta^{13}C_{carb}$ values and f_{org} remained relatively constant for hundreds of millions of years. This onset of stability is consistent with the idea that conditions surrounding the proposed superplume event actually stabilized the relative rates of burial of organic and carbonate carbon and thereby dampened large excursions in $\delta^{13}C_{carb}$. For example, the sea level rise

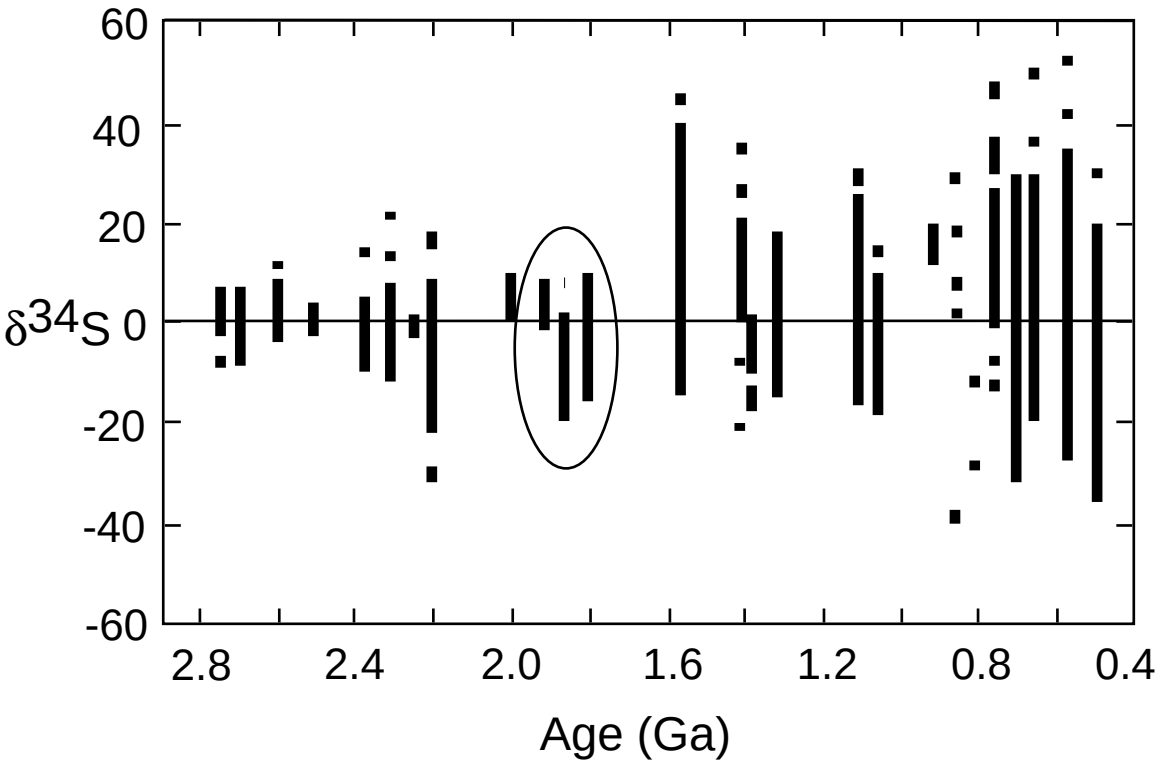

Figure 7. Sulfur isotopic composition ($\delta^{34}S_{Sred}$) of Proterozoic sedimentary sulfides versus age. The oval encloses data representing the time period of a 1.9-Ga superplume event and its aftermath. Adapted from *Knoll and Canfield* [1998].

associated with a superplume event could have flooded restricted basins, coupling them more strongly to the global ocean. Increased thermal inputs of CO_2 would have mitigated any local limitations in the supply of CO_2 within biologically productive zones, limitations that might otherwise have led to very positive $\delta^{13}C_{carb}$ values [*Melezhik et al.*, 1999].

[31] The range of δ_{Sred} values increased between 2.5 and 2.2 Ga and is consistent with an increase in seawater sulfate levels [*Knoll and Canfield*, 1998] (Figure 7). Because bacterial sulfate reduction utilizes ^{32}S preferentially over ^{34}S [*Harrison and Thode*, 1958], sedimentary sulfides typically have lower $\delta^{34}S$ values than their coeval sulfates. Isotopic mass balance considerations require that the weighted average of the $\delta_{SO4=}$ and δ_{Sred} values of sulfur species being buried must equal δ_{Sin}, which is typically 0 (see above). Between 1.9 and 1.8 Ga (circled data, Figure 7), δ_{Sred} values become more negative, indicating both that a substantial sulfate reservoir existed and that the burial rate of sulfate increased relative to that of sulfide during that time interval. This isotopic trend is consistent with the observed peak in the distribution of sulfate evaporites between 1.8 and 1.6 Ga (Figure 5).

[32] The carbon and sulfur isotope trends in Figures 6 and 7 are consistent with a high sea level stand at 1.9 Ga. This is followed by a sea level decline and a decline in platform sedimentation in favor of shallow-to-emergent coastal environments that accumulated more oxidized,

Table 2. Results of Cross-Correlation Analysis of Time Series of Black Shales, Intracratonic Sediments, and CIA for Rocks of >600 Ma[a]

Time Series	Delay, Myr	Correlation Coefficent	Confidence Level, %
CIA versus sediment	31	0.76	98.0
CIA versus sediment wt 1	39	0.79	98.0
CIA versus sediment wt 2	1099	0.84	99.9
Black shale with sediment	6	0.89	99.9
Black shale with sediment wt 1	5	0.82	99.9
Black shale with sediment wt 2	16	0.79	99.8
Black shale wt 1 with sediment	2	0.75	98.0
Black shale wt 1 with sediment wt 1	42	0.71	96.0
Black shale wt 1 with sediment wt 2	1280	0.64	82.0
Black shale wt 2 with sediment	2	0.79	99.7
Black shale wt 2 with sediment wt 1	125	0.76	99.1
Black shale wt 2 with sediment wt 2	1275	0.67	87.0

[a]Black shales are weighted according to the total thickness of the black shale (black shale weight (wt) 1) and the overall proportion of black shale in a shale sequence (black shale weight 2). Intracratonic sediments are weighted according the surface area of the sediments (sediment weight 1) and the restored surface area of sediments (sediment weight 2). The primary peak heights in the time series are related to the errors in the ages of black shale and intracratonic sediment. Thus well-dated sequences have higher peak heights than poorly dated sequences. The significance level of each correlation coefficient is calculated from 1000 simulations with random numbers of the correlation of each time series with a randomly generated time series with the same spectral characteristics [*Isley and Abbott*, 1998]. Time differences are derived from shifting one time series relative to the other in time until the highest possible correlation between the two time series is achieved.

evaporitic (sulfate) sedimentation. This view is corroborated by the decline, from 1.9 to 1.7 Ga, in stromatolite diversity and in the abundance of preserved banded iron formation and black shale and by declining δ_{Sred} values. The trend toward greater rates of sulfate deposition between 1.8 and 1.7 Ga is indicated both by increased abundance of platform sulfate-rich evaporites and generally lower δ_{Sred} values.

10. Cross-Correlation Analysis

[33] During superplume events at 480, 280, and 100 Ma, sea level rose and platform-type sedimentation became widespread [*Larson*, 1991b]. Thus, in the Precambrian we should also expect continental inundation to accompany superplume events. However, the view that Precambrian continents were flooded during superplume events presupposes either that plate motion rates increased greatly during Precambrian superplume events or that large volumes of thick oceanic plateaus were formed within ocean basins. Both types of events are difficult to document directly, either from paleomagnetic data or from geochemical studies. Furthermore, the elevation of continents during supercontinent formation might produce a reduction in continental surface area that would counteract plume-related decreases in the volume of the ocean basins. Therefore a cross-correlation analysis of time series of black shales, CIA, and intracratonic sediments is a first-order test of the idea that Precambrian superplumes either accelerated plate motions and/or created large volumes of thick oceanic plateaus.

[34] *Condie et al.* [2000] report a high correlation between the abundance of black shale and a high chemical index of alteration (CIA) in the Precambrian record. Cross-correlation analyses of abundance of black shale and intracratonic sediment have correlation coefficients with confidence levels between 87 and 99.9% (Table 2). Six out of nine of the cross correlations have confidence levels of 98% or higher, with best fitting time differences of 42 Myr or less. These

time differences are the number of years subtracted from (or added to) the ages in the first time series in order to produce the highest possible correlation between the first and second time series. Because the mean error of the sediment ages is 62 Myr, these time differences are effectively zero. Thus the deposition of black shale and intracratonic sediment is highly correlated during the Proterozoic. The cross correlations between the time series of CIA and intracratonic sediment abundance have confidence levels of 98–99.9%. Two out of three of the cross correlations have best fit time differences of 39 Myr, which again is less than the mean error (62 Myr) and, hence, effectively zero time difference. Thus high levels of atmospheric CO_2 and deposition of platform sediments are highly correlated during the Proterozoic. Overall, these results suggest that Proterozoic superplume events were associated with either accelerations in plate motion and/or formation of large volumes of oceanic plateaus.

11. Discussion and Conclusions

[35] Although the results of this study support the existence of a superplume event at 1.9 Ga, they do not prove the existence of such an event. Consistent with a superplume event at this time are the following: (1) high sea level as inferred from the relative abundance of intracratonic, passive margin, and platform sediments; (2) a relatively high abundance of black shale; (3) a peak in CIA (chemical index of alteration) in shale implying unusually warm paleoclimates; (4) a peak in the abundance of BIF; (5) a peak in the abundance of shallow marine phosphate deposits; and (6) a peak in the number of reported occurrences and in the diversity of stromatolites. Although any one of these observations may be explained by different processes, it is the coincidence of all of them at 1.9 Ga that is the most compelling evidence for a superplume event [*Condie et al.*, 2000].

[36] The peak in distribution of shallow marine sediments at 1.9 Ga suggests a corresponding high in sea level. If this reflects a superplume event, a drop in sea level during the interval of ~1.85–1.7 Ga may be due to supercontinent formation, which followed the superplume event [*Condie*, 2000b]. Increased black shale deposition and preservation at 1.9 Ga is due primarily to anoxia driven onto stable continental shelves. The black shale and CIA peaks at 1.9 Ga may reflect introduction of massive amounts of CO_2 into the atmosphere-ocean system, increasing depositional rates of carbon and increasing global warming. Such a massive injection of CO_2 into the atmosphere is again consistent with a superplume event [*Condie et al.*, 2000]. The absence of major carbon isotope anomalies in seawater at 1.9 Ga indicates that even though absolute burial rates of both reduced and oxidized carbon were accelerated at this time, their relative burial rates remained similar to those observed throughout most of the geologic record, including today [*Condie et al.*, 2000].

[37] Increased BIF and marine phosphate deposition at 1.9 Ga also may be due to a superplume event. Increased rates of deposition of these sediments may be due to increased input of iron and phosphorus into deep anoxic oceans by submarine hydrothermal activity related to a superplume event, followed by upwelling (or spreading of hydrothermal plumes) into shallow, oxidizing seas on continental shelves. The slightly low $^{87}Sr/^{86}Sr$ isotope ratios in seawater at 1.9 Ga may reflect increased mantle input of Sr from a superplume event, whereas higher ratios at 1.85–1.75 Ga reflect increased input of continental Sr from a growing supercontinent. The fact that a superplume event at 1.9 Ga did not significantly decrease seawater Sr isotope ratios may be due to the large volume of continental crust formed at 2.7 Ga, which continued to supply significant amounts of continental Sr to the oceans, thus buffering the effect

of mantle Sr related to the superplume event. A peak in reported occurrences and diversity of stromatolites in general and microdigitate stromatolites at ~1.9 Ga requires seawater on continental shelves that was greatly oversaturated in $CaCO_3$ and warm climates. Both of these observations are consistent with high sea level stands and enhanced CO_2 input into the oceans from submarine volcanism and hydrothermal vents accompanying a 1.9-Ga superplume event. The first massive sulfate evaporites in the geologic record at 1.8–1.6 Ga reflect oxidizing conditions and greater availability of Ca^{++} ions as carbonate deposition declined during superplume waning.

Acknowledgments

[38] The authors greatly appreciate the help of Dustin Smyth in compiling and synthesizing the sediment data used in estimating Proterozoic sea levels. We also acknowledge the NASA Exobiology Program and the NASA Astrobiology Institute. This is Lamont-Doherty Earth Observatory contribution 6114. The paper was substantially improved by in-depth reviews by Hubert Staudigel and two anonymous reviewers.

References

Alford, D. E., Geology and geochemistry of the Hembrillo Canyon Succession, San Andres Mountains, Sierra and Dona Ana Counties, New Mexico, M.S. thesis, N. M. Inst. of Min. and Technol., Socorro, 1987.

Ambrose, G. J., R. B. Flint, and A. W. Webb, Precambrian and Paleozoic geology of the Peake and Denison Ranges, *Bull. Geol. Surv. South Aust.*, *50*, 1981.

Argast, S., and T. W. Donnelly, Compositions and sources of metasediments in the upper Dharwar Supergroup, South India, *J. Geol.*, *94*, 215–231, 1986.

Arndt, N., Why was flood volcanism on submerged continental platforms so common in the Precambrian?, *Precambrian. Res.*, *97*, 155–164, 1999.

Asmerom, Y., et al., Strontium isotopic variations of Neoproterozoic seawater: Implications for crustal evolution, *Geochim. Cosmochim. Acta*, *55*, 2883–2894, 1991.

Aspler, L. B., and J. R. Chiarenzelli, Initiation of ~2.45–2.1 Ga intracratonic basin sedimentation of the Hurwitz Group, Keewatin Hinterland, Northwest Territories, Canada, *Precambrian Res.*, *81*, 265–297, 1997.

Awramik, S. M., The history and significance of stromatolites, in *Early Organic Evolution: Implications for Mineral and Energy Resources*, edited by M. Schidlowski, pp. 435–449, Springer-Verlag, New York, 1992.

Babinski, M., F. Chemale Jr., and W. R. Van Schmus, The Pb/Pb age of the Minas Supergroup carbonate rocks, Quadrilatero Ferrifero, Brazil, *Precambrian Res.*, *72*, 235–245, 1995.

Barley, M. E., A. L. Pickard, and P. J. Sylvester, Emplacement of a large igneous province as a possible cause of BIF 2.45 Ga, *Nature*, *385*, 55–58, 1997.

Barron, E. J., P. J. Fawcett, W. H. Peterson, D. Pollard, and S. L. Thompson, A simulation of mid-Cretaceous climate, *Paleogeography*, *10*, 953–962, 1995.

Berner, R. A., Burial of organic carbon and pyrite sulfur in sediments over Phanerozoic time: A new theory, *Geochim. Cosmochim. Acta*, *47*, 855–862, 1983.

Berner, R. A., A new look at the long-term carbon cycle, *GSA Today*, *9*(11), 1–6, 1999.

Blake, D. H., and A. J. Stewart, Stratigraphic and tectonic framework, Mt. Isa Inlier, *Bull. Bur. Miner. Resour. Geol. Geophys. Aust.*, *243*, 1–11, 1992.

Blake, D. H., A. J. Stewart, I. P. Sweet, and I. G. Hone, Geology of the Proterozoic Davenport province, central Australia, *Bull. Bur. Miner. Resour. Geol. Geophys. Aust.*, *226*, 1987.

Bonhomme, M. G., et al., Radiochronological age and correlation of Proterozoic sediments in Brazil, *Precamrian. Res.*, *18*, 103–118, 1982.

Brasier, M. D., and J. F. Lindsay, A billion years of environmental stability and the emergence of eukaryotes: New data from northern Australia, *Geology*, *26*, 555–558, 1998.

Brito Neves, B., and U. G. Cordani, Tectonic evolution of South America during the Late Proterozoic, *Precambrian Res.*, *53*, 23–40, 1991.

Brookfield, M. E., Problems in applying preservation, facies and sequence modes to Sinian glacial sequences in Australia and Asia, *Precambrian Res.*, *70*, 113–143, 1994.

Buick, R., D. J. Des Marais, and A. H. Knoll, Stable isotopic compositions of carbonates from the Mesoproterozoic Bangemall Group, northwestern Australia, *Chem. Geol.*, *123*, 153–171, 1995.

Buick, I. S., R. Uken, R. L. Gibson, and T. Wallmach, High-^{13}C Paleoproterozoic carbonates from the Transvaal Supergroup, South Africa, *Geology*, *26*, 785–878, 1998.

Cahen, L., and N. J. Snelling, *The Geochronology and Evolution of Africa*, Clarendon, Oxford, England, 1984.

Campbell, F. H., Stratigraphy and sedimentation in the Helikian Elu Basin and Hiukitak Platform, Bathhurst

Inlet-Melville Sound, Northwest Territories, *Pap. Geol. Surv. Can.*, *79-8*, 1979.

Canfield, D. E., A new model for Proterozoic ocean chemistry, *Nature*, *396*, 450–453, 1998.

Chakrabarti, A., Traces and dubiotraces: Examples from the so-called Late Proterozoic siliclastic rocks of the Vindhyan Supergroup around Maihar, India, *Precambrian Res.*, *47*, 141–153, 1990.

Chandler, F. W., and R. R. Parrish, Age of the Richmond Gulf Group and implications for rifting in the Trans-Hudson Orogen, Canada, *Precambrian Res.*, *44*, 277–288, 1989.

Chaudhuri, A. K., et al., Stratigraphy of the Penganga Group around Adilabad, Andhra Pradesh, *J. Geol. Soc. India*, *34*, 291–302, 1989.

Cheney, E. S., and D. Twist, The Waterberg basin-a re-appraisal, *Trans. Geol. Soc. S. Afr.*, *89*, 353–360, 1986.

Cheney, E. S., and H. de la R. Winter, The Late Archean to Mesoproterozoic major unconformity-bounded units of the Kaapvaal province of southern Africa, *Precambrian Res.*, *74*, 203–223, 1995.

Cingolani, C. A., and M. G. Bonhomme, Geochronology of La Tinta upper Proterozoic sedimentary rocks, Argentina, *Precambrian Res.*, *18*, 119–132, 1982.

Clauer, N., C. R. Caby, J. Daniel, and T. Roland, Geochronology of sedimentary and metasedimentary Precambrian rocks of the West African craton, *Precambrian Res.*, *18*, 53–71, 1982.

Collins, P. L. F., and I. R. McDonald, A Proterozoic sediment-hosted polymetallic epithermal deposit at Abra in the Jilawarra sub-basin of the central Bangemall basin, Western Australia, *Geol. Soc. Aust. Abstr.*, *37*, 68–69, 1994.

Condie, K. C., Episodic continental growth and supercontinents: a mantle avalanche connection?, *Earth Planet. Sci. Lett.*, *163*, 97–108, 1998.

Condie, K. C., Episodic continental growth models: Afterthoughts and extensions, *Tectonophysics*, *322*, 153–162, 2000a.

Condie, K. C., Continental growth during formation of Rodinia at 1.35–0.9 Ga, *Gondwana Res.*, in press, 2000b.

Condie, K. C., Continental growth during a 1.9-Ga superplume event, *Geol. Soc. Am. Abstr. Programs*, *32*(7), 314–315, 2000c.

Condie, K. C., and D. J. Des Marais, Black shales and paleoweathering: Response to mantle plume events and the supercontinent cycle, *Geol. Soc. Am. Abstr. Programs*, *31*(7), A-325, 1999.

Condie, K. C., M. Wilks, O. M. Rosen, and V. L. Zlobin, Geochemistry of metasediments from the Precambrian Hapschan series, eastern Anabar Shield, Siberia, *Precambrian Res.*, *50*, 37–47, 1991.

Condie, K. C., D. J. Des Marais, and D. Abbott, Precambrian superplumes and supercontinents: A record in black shales, carbon isotopes, and paleoclimates?, *Precambrian Res.*, in press, 2000.

Cook, P. J., and M. W. McElhinny, A reevaluation of the spatial and temporal distribution of sedimentary phosphate deposits in the light of plate tectonics, *Econ. Geol.*, *74*, 315–330, 1979.

Cook, P. J., and J. H. Shergold, Phosphorus, phosphorites and skeletal evolution at the Precambrian-Cambrian boundary, *Nature*, *308*, 231–236, 1984.

Cook, P. J., and J. H. Shergold, Proterozoic and Cambrian phosphorites: Nature and origin, in *Phosphate Deposits of the World*, edited by P. J. Cook and J. H. Shergold, pp. 369–386, Cambridge Univ. Press, New York, 1986.

Des Marais, D. J., Isotopic evolution of the biogeochemical carbon cycle during the Proterozoic Eon, *Org. Geochem.*, *27*, 185–193, 1997.

Des Marais, D. J., H. Strauss, R. E. Summons, and J. M. Hayes, Carbon isotope evidence for the stepwise oxidation of the Proterozoic environment, *Nature*, *359*, 605–609, 1992.

Dirks, P. H., and A. R. Norman, Physical sedimentation processes on a Mid-Proterozoic shelf: The Reynolds Range Group, Arunta block, central Australia, *Precambrian Res.*, *59*, 225–241, 1992.

Doe, M. F., and K. E. Karlstrom, Structural geology of an Early Proterozoic foreland thrust belt, Mazatzal Mountains, Arizona, *Ariz. Geol. Soc. Dig.*, *19*, 181–192, 1991.

Donaldson, J. A., and B. D. Ricketts, Beachrock in Proterozoic dolostone of the Belcher Islands, Northwest Territories, Canada, *J. Sediment. Petrol.*, *49*, 1287–1294, 1979.

Eriksson, P. G., Sea level changes and the continental freeboard concept: General principles and application to the Precambrian, *Precambrian Res.*, *97*, 143–154, 1999.

Eriksson, P. G., and C. W. Clendenin, A review of the Transvaal sequence, *South Africa, J. Afr. Earth Sci.*, *10*, 101–116, 1990.

Eriksson, P. G., R. Mazumder, S. Sarkar, P. K. Bose, W. Altermann, and R. van der Merwe, The 2.7–2.0 Ga volcano-sedimentary record of Africa, India and Australia: Evidence for global local changes in sea level and continental freeboard, *Precambrian Res.*, *97*, 269–302, 1999.

Fairchild, I. J., and M. J. Hambrey, The Vendian succession of NE Spitsbergen: Petrogenesis of a dolomite-tillite association, *Precambrian Res.*, *26*, 111–167, 1984.

Fairchild, I. J., and M. J. Hambrey, Vendian basin evolution in East Greenland and NE Svalbard, *Precambrian Res.*, *73*, 217–233, 1995.

Fairchild, T. R., et al., Recent discoveries of Proterozoic microfossils in south-central Brazil, *Precambrian Res.*, *80*, 125–152, 1996.

Fedo, C. M., G. M. Young, and H. W. Nesbitt, Paleoclimatic control on the composition of the Paleoproterozoic Serpent Formation, Huronian Supergroup, Canada: A greenhouse to icehouse transition, *Precambrian Res.*, *86*, 201–223, 1997.

Galer, S. J. G., Interrelationships between continental freeboard, tectonics and mantle temperature, *Earth Planet. Sci. Lett.*, *105*, 214–228, 1991.

Gibbs, A. K., and C. N. Barron, *The Geology of the Guiana Shield*, Oxford Univ. Press, New York, 1993.

Goodwin, A. M., *Precambrian Geology*, 666 pp., Academic, San Diego, Calif., 1991.

Greenberg, J. K., and B. A. Brown, Lower Proterozoic volcanic rocks and their setting in the southern Lake Superior District, *Mem. Geol. Soc. Am.*, *160*, 1984a.

Greenberg, J. K., and B. A. Brown, Cratonic sedimentation during the Proterozoic: An anorogenic connection in the Wisconsin and the Upper Midwest, *J. Geol.*, *92*, 159–171, 1984b.

Greff-Lefftz, M., and H. Legros, Core rotational dynamics and geological events, *Science*, *286*, 1707–1709, 1999.

Gresse, P. G., and G. J. B. Germs, The Nama foreland basin: Sedimentation, major unconformity bounded sequences and multisided active margin advance, *Precambrian Res.*, *63*, 247–272, 1993.

Grotzinger, J. P., and J. F. Kasting, New constraints on Precambrian ocean composition, *J. Geol.*, *101*, 235–243, 1993.

Grotzinger, J. P., and A. H. Knoll, Stromatolites in Precambrian carbonates: Evolutionary mileposts or environmental dipsticks?, *Annu. Rev. Earth Planet. Sci.*, *27*, 313–358, 1999.

Gurnis, M., Phanerozoic marine inundation of continents driven by dynamic topography above subducting slabs, *Nature*, *364*, 589–593, 1993.

Hall, S. M., and J. Veizer, Geochemistry of Precambrian carbonates, VII, Belt Supergroup, Montana and Idaho, USA, *Geochim. Cosmochim. Acta*, *60*, 667–677, 1996.

Hardebeck, J., and D. L. Anderson, Eustasy as a test of a Cretaceous superplume hypothesis, *Earth Planet. Sci. Lett.*, *137*, 101–108, 1996.

Harrison, A. G., and H. G. Thode, Mechanisms of the bacterial reduction of sulfate from isotope fractionation studies, *Trans. Faraday Soc.*, *53*, 84–92, 1958.

Heaman, L. M., and J. P. Grotzinger, 1.08 Ga diabase sills in the Pahrump Group, California: Implications for development of the Cordilleran miogeocline, *Geology*, *20*, 637–664, 1992.

Heiskanen, K. I., Early Proterozoic sedimentary basins of the Baltic shield, *Inf. Circ. Minn. Geol. Surv.*, *34*, 1991.

Hills, F. A., and R. S. Houston, Early Proterozoic tectonics of the central Rocky Mountains, North America, *Contrib. Geol.*, *17*(2), 89–109, 1979.

Hoffman, P. F., United plates of America, the birth of a craton: Early Proterozoic assembly and growth of Laurentia, *Annu. Rev. Earth Planet. Sci.*, *16*, 543–603, 1988.

Hofmann, H. J., Synopsis of Precambrian fossil occurrences in North America, in *The Geology of North America*, vol. C-1, chap. 4, pp. 273–293, Geol. Soc. of Am., Boulder, Colo., 1998.

Holm, D. K., The Flambeau deformation and thermal front in northwest Wisconsin and its bearing on the minimum age of Proterozoic cratonic quartzites, *Geol. Soc. Am. Abstr. Programs*, *29*(6), A-465, 1997.

Holser, W. T., M. Schidlowski, F. T. Mackenzie, and J. B. Maynard, Geochemical cycles of carbon and sulfur, in *Chemical Cycles in the Evolution of the Earth*, edited by C. B. Gregor et al., pp. 105–173, John Wiley, New York, 1988.

Hynes, A., and R. D. Gee, Geological setting and petrochemistry of the Narracoota volcanics, Capricorn orogen, W. Australia, *Precambrian Res.*, *31*, 107–132, 1986.

Isley, A. E., Hydrothermal plumes and the delivery of iron to BIF, *J. Geol.*, *103*, 169–185, 1995.

Isley, A. E., and D. H. Abbott, Plume-related mafic volcanism and the deposition of banded iron formation, *J. Geophys. Res.*, *104*, 15,461–15,477, 1999.

Jefferson, C. W., and G. M. Young, Late Proterozoic orange-weathering stromatolite biostrome, MacKenzie Mountains and western Arctic Canada, *Mem. Can. Soc. Pet. Geol.*, *13*, 72–80, 1989.

Kale, V. S., and V. G. Phansalkar, Purana basins of peninsular India: A review, *Basin Res.*, *3*, 1–36, 1991.

Karhu, J. A., and H. D. Holland, Carbon isotopes and the rise of atmospheric oxygen, *Geology*, *24*, 867–870, 1996.

Karlstrom, K. E., A. J. Flurkey, and R. S. Houston, Stratigraphy and depositional setting of the Proterozoic Snowy Pass Supergroup, southeastern Wyoming: Record of an Early Proterozoic Atlantic-type cratonic margin, *Geol. Soc. Am. Bull.*, *94*, 1257–1274, 1983.

Kaufman, A. J., and A. H. Knoll, Neoproterozoic variations in the C-isotopic composition of seawater: Stratigraphic and biogeochemical implications, *Precambrian Res.*, *73*, 27–49, 1995.

Kerr, A. C., Lithospheric thinning during the evolution of continental large igneous provinces, *Geology*, *22*, 1027–1030, 1994.

Kerr, A. C., Oceanic plateau formation: A cause of mass extinction and black shale deposition around the Cenomanian-Turonian boundary?, *J. Geol. Soc. London*, *155*, 619–626, 1998.

Klein, C., and N. J. Beukes, Time distribution, stratigraphy, and sedimentologic setting and geochemistry of Precambrian iron formations, in *The Proterozoic Biosphere: A Multidisciplinary Study*, pp. 139–146, Cambridge Univ. Press, New York, 1992.

Knight, I., and C. W. Morgan, The Aphebian Ramah Group, Northern Labrador, *Pap. Geol. Surv. Can.*, *81-10*, 313–330, 1981.

Knoll, A. H., and D. E. Canfield, Isotopic inferences on early ecosystems, in *Isotope Paleoebiology and Paleoecology*, edited by R. D. Norris and R. M. Corfield, *Paleontol. Soc. Pap.*, *4*, 212–243, 1998.

Kotzer, T. G., and T. K. Kyser, Petrogenesis of the Proterozoic Athabasca Basin, northern Saskatchewan, Canada, and its relation to diagenesis, hydrothermal uranium mineralization and paleohydrogeology, *Chem. Geol.*, *120*, 45–89, 1995.

Kukla, P. A., and I. G. Stanistreet, Record of the Damaran hochland accretionary prism in central Namibia: Refutation of an ensialic origin of a Later Proterozoic orogenic belt, *Geology*, *19*, 473–476, 1991.

Kumar, S., Megafossils from the Mesoproterozoic Rhotas Formation, Katni area, central India, *Precambrian Res.*, *72*, 171–184, 1995.

Larson, R. L., Latest pulse of Earth: Evidence for a mid-Cretaceous superplume, *Geology*, *19*, 547–550, 1991a.

Larson, R. L., Geological consequences of superplumes, *Geology*, *19*, 963–966, 1991b.

Ledru, P., J. E. N'dong, and V. Johan, Structural and metamorphic evolution of the Gabon orogenic belt: Collision tectonics in the lower Proterozoic, *Precambrian Res.*, *44*, 227–240, 1989.

Ledru, P., J. P. Milesi, V. Johan, P. Sabate, and H. Maluski, Foreland basins and gold-bearing conglomerates: A new model for the Jacobina basin (Sao Francisco craton, Brazil), *Precambrian Res.*, *86*, 155–176, 1997.

Li, X., and M. T. McCulloch, Secular variation in the Nd isotopic composition of Neoproterozoic sediments form the southern margin of the Yangtze block: Evidence for a Proterozoic continental collision in the SE China, *Precambrian Res.*, *76*, 67–76, 1996.

Link, P. K., et al., Middle and Late Proterozoic Rocks of the Western U.S. Cordillera, Colorado Plateau, and Basin and Range Province, in *The Geology of North America*, vol. C-2, *Precambrian: Conterminous U. S.*, edited by J. C. Reed Jr. et al., pp. 463–595, Geol. Soc. of Am., Boulder, Colo., 1993.

Litherland, M., et al., The geology and mineral resources of the Bolivian Precambrian shield, *Overseas Mem. Br. Geol. Surv.*, *9*, 145 pp., 1986.

Lithgow-Bertelloni, C., and P. G. Silver, Dynamic topography, plate driving forces and the African superswell, *Nature*, *395*, 269–272, 1998.

Machado, N., A. Schrank, C. M. Noce, and G. Gauthier, Ages of detrital zircon from Archean-Paleoproterozoic sequences: Implications for greenstone belt setting and evolution of a Transamazonian foreland basin in Quadrilatero Ferrifer, SE Brazil, *Earth Planet. Sci. Lett.*, *141*, 259–276, 1996.

Manikyamba, C., and S. M. Naqvi, Geochemistry of Fe-Mn formations of the Archean Sandur schist belt, India: Mixing of clastic and chemical processes at a shallow shelf, *Precambrian Res.*, *72*, 69–95, 1995.

Marshak, S., and F. F. Alkmim, Proterozoic contraction/extension tectonics of the southern Sao Francisco region Minas Gerais, Brazil, *Tectonics*, *8*, 555–571, 1989.

Master, S., Stratigraphy, tectonic setting, and mineralization of the Early Proterozoic Magondi Supergroup, Zimbabwe: A review, *Univ. Witwatersrand, Econ. Geol. Res. Unit Inf. Circ.*, *238*, 75 pp., 1991.

Meijerink, A. M. J., D. P. Rao, and J. Rupke, Stratigraphic and structural development of the Precambrian Cuddapah basin, SE India, *Precambrian Res.*, *26*, 57–104, 1984.

Melezhik, V. A., A. E. Fallick, V. V. Makarikhin, and V. V. Lyubtsov, Links between Paleoproterozoic paleogeography and rise and decline of stromatolites: Fennoscandian shield, *Precambrian Res.*, *82*, 311–348, 1997.

Melezhik, V. A., A. E. Fallick, P. V. Medvedev, and V. V. Makarikhin, Extreme $^{13}C_{carb}$ enrichment in ca. 2.0 Ga magnesite-stromatolite-dolomite- 'red beds' association in a global context: A case for the world-wide signal enhanced by a local environment, *Earth Sci. Rev.*, *48*, 71–120, 1999.

Mendelsohn, F., Precambrian geology of Zaire and Zambia, in *Precambrian of the Southern Hemisphere*, edited by D. R. Hunter, pp. 721–738, Elsevier Sci., New York, 1981.

Mirota, M. D., and J. Veizer, Geochemistry of Precambrian carbonates, VI, Aphebian Albanel Formation, Quebec, *Geochim. Cosmochim. Acta*, *58*, 1735–1745, 1994.

Misi, A., and J. Veizer, Neoproterozoic carbonate sequence of the Una Group, Irece basin: Chemostratigraphy, age, and correlations, *Precambrian Res.*, *89*, 87–100, 1998.

Moore, J. M., Jr., and P. H. Thompson, The Flinton Group: A Late Precambrian metasedimentary succession in the Grenville Province of eastern Ontario, *Can. J. Res.*, *17*, 1685–1707, 1980.

Myers, J. S., R. D. Shaw, and I. M. Tyler, Tectonic evolution of Proterozoic Australia, *Tectonics*, *15*, 1431–1446, 1997.

Narbonne, G. M., and J. D. Aitken, Neoproterozoic of the Makenzie Mountains, northwestern Canada, *Precambrian Res.*, *73*, 101–121, 1995.

Needham, R. S., P. G. Stuart-Smith, and R. W. Page, Tectonic evolution of the Pine Creek inlier, Northern Territory, *Precambrian Res.*, *40/41*, 543–564, 1988.

Nesbitt, H. W., and G. M. Young, Early Proterozoic climates and plate motions inferred from major element chemistry of lutites, *Nature*, *299*, 715–717, 1982.

Nesbitt, H. W., G. M. Young, S. M. McLennan, and R. R. Keays, Effects of chemical weathering and sorting on the petrogenesis of siliciclastic sediment, with implications for provenance studies, *J. Geol.*, *104*, 525–542, 1996.

Nutman, A. P., and K. Ehlers, Evidence for multiple Paleoproterozoic thermal events and magmatism adjacent to the Broken Hill Pb-Zn-Ag orebody, *Aust. Precambrian Res.*, *90*, 203–238, 1998.

Ojakangas, R. W., and G. B. Morey, Keweenawan prevolcanic quartz sandstones and related rocks of the Lake Superior region, *Mem. Geol. Soc. Am.*, *156*, 85–96, 1982.

Pagel, H. O., J. Borshoff, and R. Coles, Veinlike uranium deposits in the Rum Jungle area: Geological setting and relevant exploration features, in *Darwin Conference*, *1984*, pp. 225–238, Aust. Inst. of Min. and Metal., Victoria, 1984.

Pirajno, F., L. Bagas, C. P. Swager, S. Occhipinti, and N. G. Adamides, Reappraisal of the stratigraphy of the Glengarry basin, Western Australia, *Annu. Rev. Geol. Surv. West. Aust.*, *1995–1996*, 1996.

Powell, D. M., W. V. Preiss, C. G. Gatehouse, B. Krapez, and Z. X. Li, South Australian record of a Rodinian epicontinental basin and its mid-Neoproterozoic breakup to form the Paleo-Pacific ocean, *Tectonophysics*, *237*, 113–140, 1994.

Ramaekers, P., Hudsonian and Helikean basins of the Athabasca Region, northern Saskatchewan, *Pap. Geol. Surv. Can.*, *81-10*, 219–233, 1981.

Rawlings, D. J., Stratigraphic resolution of a multiphase intracratonic basin system: The McArthur Basin, N. Australia, *Aust. J. Earth Sci.*, *46*, 703–723, 1999.

Rivers, T., Lithotectonic elements of the Grenville Province: Review and tectonic implications, *Precambrian Res.*, *86*, 117–154, 1997.

Robb, L. J., D. W. Davis, and S. L. Kamo, U-Pb ages on single detrital zircon grains from the Witwatersrand basin, South Africa: Constraints on the age of sedimentation and on the evolution of granites adjacent to the basin, *J. Geol.*, *98*, 311–328, 1990.

Rosen, O. M., K. C. Condie, L. M. Natapov, and A. D. Nozhkin, Archean and Early Proterozoic evolution of the Siberian craton: A preliminary assessment, in *Archean Crustal Evolution*, edited by K. C. Condie, pp. 411–459, Elsevier Sci., New York, 1994.

Semikhatov, M. A., and M. E. Raaben, Dynamics of the global diversity of Proterozoic stromatolites, article II, *Stratigr. Geol. Correlation*, *4*, 24–50, 1996.

Sergeev, V. N., Microfossils in chertts from the Middle Riphean Avzyan Formation, southern Ural Mountains, Russian Federation, *Precambrian Res.*, *65*, 231–254, 1994.

Sergeev, V. N., A. H. Knoll, and P. Y. Petrov, Paleobiology of the Mesoproterozoic-Neoproterozoic transition: The Sukhaya Tunguska Formation, Turukhansk uplift, Siberia, *Precambrian Res.*, *85*, 201–239, 1997.

Sheraton, J. W., R. J. Tingley, L. P. Black, L. A. Offe, and D. J. Ellis, Geology of an unusual Precambrian high-grade metamorphic terrane: Enderby Land and western Kemp Land, Antarctica, *Bull. Bur. Miner. Resour. Geol. Geophys. Aust.*, *223*, 1987.

Simonson, B. M., and S. W. Hassler, Was the deposition of large Precambrian iron formations linked to major marine transgression?, *J. Geol.*, *104*, 665–676, 1996.

Sims, P. K., et al., The Lake Superior Region and the Trans-Hudson orogen, in *The Geology of North America*, vol. C-2, *Precambrian: Conterminous U. S.*, edited by J. C. Reed Jr. et al., pp. 11–120, Geol. Soc. of Am., Boulder, Colo., 1993.

Smith, L. H., A. J. Kaufman, A. H. Knoll, and P. K. Link, Chemostratigraphy of predominantly siliciclastic Neoproterozoic successions: A case study of the Pocatello Formation and the Lower Brigham Group, Idaho, USA, *Geology*, *131*, 301–314, 1994.

Soegaard, K., and K. A. Eriksson, Origin of thick, first-cycle quartz arenite successions: Evidence from the 1.7 Ga Ortega Group, northern New Mexico, *Precambrian Res.*, *43*, 129–141, 1989.

Sun, D., W. Hu, M. Tang, F. Zhao, and K. C. Condie, Origin of Late Archean and Early Proterozoic rocks and associated mineral deposits from the Zhongtiao Mountains, east-central China, *Precambrian Res.*, *47*, 287–306, 1990.

Sweet, I. P., The Precambrian geology of the Victoria River region, N. Territory, *Bull. Bur. Miner. Resour. Geol. Geophys. Aust.*, *168*, 1977.

Tankard, A. J., et al., *Crustal Evolution of Southern Africa*, 523 pp., Springer-Verlag, New York, 1982.

Taylor, S. R., and S. M. McLennan, *The Continental Crust: Its Composition and Evolution*, 312 pp., Blackwell Sci., Malden, Mass., 1985.

Teixeira, W., C. C. G. Tassinari, U. G. Cordani, and K. Kawashita, A review of the geochronology of the Amazonian craton: Tectonic implications, *Precambrian Res.*, *42*, 213–227, 1989.

Thorne, A. M., and D. B. Seymour, Geology of the Ashburton basin, Western Australia, *Bull. Geol. Surv. West. Aust.*, *139*, 1991.

Trendall, A. F., Hamersley basin, in *Iron Formations:*

Facts and Problems, edited by A. F. Trendall and R. C. Morris, pp. 69–129, Elsevier Sci., New York, 1983.

Tyler, I. M., and T. J. Griffin, Structural development of the King Leopold orogen, Kimberley region, Western Australia, *J. Struct. Geol.*, *12*, 703–714, 1990.

Unrug, R., The Mid-Proterozoic Mporokoso Group of Northern Zambia: Stratigraphy, sedimentation and regional position, *Precambrian Res.*, *24*, 99–121, 1984.

Van Schmus, W. R., Early and Middle Proterozoic history of the Great Lakes area, North America, *Philos. Trans. R. Soc. London*, *280*, 605–628, 1976.

Veizer, J., The evolving exogenic cycle, in *Chemical Cycles in the Evolution of the Earth*, edited by C. B. Gregor et al., pp. 175–219, John Wiley, New York, 1988.

Veizer, J., Strontium isotopes in seawater through time, *Annu. Rev. Earth Planet. Sci.*, *17*, 141–167, 1989.

Veizer, J., and W. Compston, $^{87}Sr/^{86}Sr$ in Precambrian carbonates as an index of crustal evolution, *Geochim. Cosmochim. Acta*, *40*, 905–914, 1976.

Veizer, J., and S. L. Jansen, Basement and sedimentary recycling, 2, Time dimension to global tectonics, *J. Geol.*, *93*, 625–643, 1985.

Verma, P. K., and R. O. Greiling, Tectonic evolution of the Aravalli orogen, NW India: An inverted Proterozoic rift basin, *Geol. Rundsch.*, *84*, 683–696, 1995.

Vidal, G., and M. Moczydlowska, The Neoproterozoic of Baltica-stratigraphy, paleobiology and general geological evolution, *Precambrian Res.*, *73*, 197–216, 1995.

Villeneuve, M., The geology of the Madina-Kouta basin and its significance for the geodynamic evolution of the western part of the West African craton during the upper Proterozoic period, *Precambrian Res.*, *44*, 305–322, 1989.

Wang, H., and X. Qiao, Proterozoic stratigraphy and tectonic framework of China, *Geol. Mag.*, *121*, 599–614, 1984.

Wiedenbeck, M., J. N. Goswami, and A. B. Roy, Stabilization of the Aravalli craton of NW India at 2.5 Ga: An ion microprobe zircon study, *Chem. Geol.*, *129*, 325–340, 1996.

Williams, I. R., Yeneena basin, *Mem. Geol. Surv. West. Aust.*, *3*, 277–282, 1990.

Winter, H. de la R., Foreland depobasin reponse of the Witwatersrand Supergroup in the Rietfontein-E Rand region: Eustatic marine parallels and tectonic continental contrast around the proximal rim, *S. Afr. J. Geol.*, *97*, 119–134, 1994.

Wright, L. A., B. W. Troxel, E. G. Williams, M. T. Roberts, and P. E. Diehl, Precambrian sedimentary environments of the Death Valley Region, Eastern California, in *Guidebook: Death Valley Region, California and Nevada*, pp. 27–35,Geol. Soc. of Am., Boulder, Colo., 1974.

Yun, Z., Stromatolitic microbiota from the Middle Proterozoic Wumishan Formation of the Ming Tombs, Beijing, China, *Precambrian Res.*, *30*, 277–302, 1985.

Zang, W., Early Neoproterozoic sequence stratigraphy and acritarch biostratigraphy, eastern Officer basin, South Australia, *Precambrian Res.*, *74*, 119–175, 1995.

Zang, W., and M. R. Walter, Late Proterozoic and Early Cambrian microfossils and biostratigraphy, northern Anhui and Jiangsu, central-eastern China, *Precambrian Res.*, *57*, 243–323, 1992.

Zunyi, Y., C. Yuqi, and W. Hongzhen, *The Geology of China*, Clarendon, Oxford, England, 1986.